Computer simulations of nematic droplets with bipolar boundary conditions

E. Berggren and C. Zannoni
Dipartimento di Chimica Fisica ed Inorganica, Università di Bologna, Viale Risorgimento 4, 40136 Bologna, Italy

C. Chiccoli, P. Pasini, and F. Semeria
Istituto Nazionale di Fisica Nucleare, Sezione di Bologna, Via Irnerio 46, 40126 Bologna, Italy
(Received 26 January 1994)

We present Monte Carlo computer simulations of model nematic droplets that mimic polymer dispersed liquid crystals (PDLC's) with bipolar boundary conditions. We investigate the orientational order and the molecular organization in these systems for various anchoring strengths and for external applied fields of different magnitude both for positive and negative susceptivity anisotropy. We report a number of simulations for system sizes from 304 to 11 752 particles and calculate powder deuterium NMR spectra and polarizing microscope textures for the various cases.

PACS number(s): 61.30.Gd, 61.30.Jf, 64.70.Md

I. INTRODUCTION

The development of polymer dispersed liquid crystals (PDLC's) [1–10] and of other confined liquid crystal systems, particularly in spherical or cylindrical environments [11–18], has opened new important possibilities in the study and application of mesophases. PDLC's are formed of micrometer or submicrometer size nematic droplets that can be prepared, by suitably choosing the polymer matrix and the preparation method, with well defined boundary conditions. The polymer-nematic interface conditions tend to influence the orientation of molecules near to the surface and the aligning effect may propagate inside the droplet. Calculation of the corresponding stable director configuration has been performed in a number of cases at the "continuum theory" level by minimizing the appropriate Frank elastic free energy [19,20]. From a microscopic point of view there will be in general a competition between the molecular orientation induced by the surface boundary conditions, the effects caused by the ordering of the liquid crystal itself due to the molecules trying to arrange themselves parallel to each other, and the disordering effect of temperature. The resulting molecular organization for a certain boundary condition will thus depend on a number of factors, including the strength of the surface interaction and the temperature. This in turn means that the organization is not easy to predict with microscopic theories and even, especially for the smaller sizes, to investigate it experimentally [19]. We have shown [21,22] that Monte Carlo simulations can be a particularly effective tool to predict the combined effect of these factors without resorting to continuum theory, whose applicability on such small scales is not to be taken for granted. In various recent papers we have investigated, using Monte Carlo simulations, the molecular organization in droplets with radial [21,22] and toroidal [23] boundary conditions. We have examined temperature and size effects and in particular [21(a)] we have considered radial boundary conditions with a rather strong anchoring energy, i.e., with a surface interaction of the same strength as that existing between the nematogen particles and we have examined the effect of changing the anchoring strength [21(b)] as well as the effect of an external applied field [22].

Another important type of organization found in PDLC's is the bipolar one, which is one of the most frequently used in applications. In this case boundary molecules are directed along the local meridians while being tangential to the surface and two point defects are created at the poles. This kind of structure has been investigated experimentally and theoretically using elastic theories [4–10,19,24]. Field effects have also been studied experimentally for bipolar droplets [25,26]. Microscopic Monte Carlo simulations of bipolar droplets have not been performed as yet. Here we wish to present such calculations for a number of relevant conditions. First we examine the case of droplets with bipolar boundary conditions with various anchoring strengths. The effect that the application of a field has on the ordering inside the droplet and the modifications that the field induces on the phase transition behavior and molecular organization will also be studied. We make contact with experimental methods by calculating NMR line shapes [22] and optical patterns for polarized light microscopy corresponding to the configurations found.

II. MODEL

We consider a lattice model of PDLC's because we are essentially interested in orientational phenomena and these are well reproduced by models with discretized positions and continuously varying orientations such as the Lebwohl-Lasher (LL) one [27,28]. In our model the

droplet is a jagged sphere $\mathcal{S}$ carved from the cubic lattice by considering all the molecules falling at a given distance from the chosen center.

The bipolar boundary conditions (BBC's) are mimicked assuming a layer of outside particles $\mathcal{G}$ having orientations tangential to the droplet surface and directed along the meridians, i.e., towards the poles. Each particle is represented by a unit vector $\mathbf{u}_i$ and the pair interaction is then assumed to be

$$U_{i,j} = -\epsilon_{ij} P_2(\cos\beta_{ij}) \qquad \text{for} \qquad i,j \in \mathcal{S} \tag{2.1}$$

and

$$U_{i,j} = -\epsilon_{ij} J P_2(\cos\beta_{ij}) \qquad \text{for} \qquad i \in \mathcal{S}, \quad j \in \mathcal{G} \tag{2.2}$$

where ϵ_{ij} is a positive constant, ϵ, for nearest neighbor particles i and j and zero otherwise, β_{ij} is the angle between the axis of the two spins ($\cos\beta_{ij} = \mathbf{u}_i \cdot \mathbf{u}_j$), and P_2 is a second-rank Legendre polynomial. We have chosen to simulate the effect of different anchoring strengths with the polymer surface by introducing a parameter J that defines the extent of coupling to the external environment; in practice the coupling between the molecules is taken to be different from that in the bulk if one of them belongs to the surface. When the interaction between sites inside and outside the droplet is the same ($J = 1$) and when, of course, the orientation of the particles outside is not frozen, the model reduces to the usual Lebwohl-Lasher model. The LL model has been extensively studied and represents the prototype for the nematic isotropic orientational phase transition. It reproduces a weakly first order transition for the bulk [28], while in a confined system with radial or tangential boundary conditions of sufficient small size the phase transition is suppressed.

As we have shown in our previous papers [21–23] these models present several advantages connected with their simplicity; in particular a large number of sites (of the order of a few thousand) can be treated while, using more "realistic" potentials, only a fairly limited sample (typically a few hundred particles) can be simulated; moreover and more importantly here, a number of different physical situations can be systematically investigated in a way that would not be possible otherwise.

The simplest way of connecting the LL model to a real molecular system is to associate each site with a single molecule. However, a lattice site could also correspond equally well to a small domain or cluster of molecules with a common orientation and a structure that is essentially the same on both sides of the transition. Such a basic building block whose local short range order is maintained above the transition was invoked some years ago [29] to rationalize the success of a simple Maier-Saupe–type mean field theory and the low nematic-isotropic transition entropy. This cluster model is supported also by the findings of a recent simulation of the more realistic Gay-Berne model [30], where the particles have ellipsoidal shape with an attractive and repulsive part and full translational freedom. In this case the short range part of the pair distribution is essentially unchanged going through the transition. From the point of view of the model the interpretation of a lattice site ("spin") as a group of molecules rather than a single one only provides a renormalization that is only important when comparison with an absolute energy (temperature) or length scale as opposed to the usual dimensionless one is attempted. In general the importance of the LL model and of similar models is clearly more in predicting behavior in relative terms, e.g., the trend of order and correlations near the transition and the transition temperature in reduced units. Here we talk of particles or even molecules as a convenient alias for lattice sites, and we will return to the details of interpretation later on when we discuss optical texture simulations. In the first part of this work we shall examine the effect of varying the anchoring strength J.

Another important problem we wish to tackle is that of the effect of an applied field on molecular organization. To do this, a suitable second-rank term is added to the Hamiltonian to keep an account of the contribution to the orientational energy due to the interaction between the particles and the external field [22,31]. We consider in this case only the anchoring strength $J = 1$, so that the overall potential energy is

$$U_N = -\sum_{\substack{i,j \\ i<j}} \epsilon_{ij} P_2(\cos\beta_{ij}) - \epsilon\xi \sum_{i=1}^{N} P_2(\cos\beta_i), \tag{2.3}$$

where N is the number of particles contained in the sphere, β_i is the angle between the field direction and the particle symmetry axis, and ξ determines the strength of the coupling to the field. This kind of potential was used some years ago to investigate the application of an external field on a nematic bulk system [31]. Recently we have studied this model in the case of nematic droplets with radial boundary conditions [22]. The applied field can in practice be an electric or a magnetic one and the parameter ξ will then depend on the appropriate susceptivity anisotropy and field strength as discussed in Ref. [22].

III. SIMULATIONS AND RESULTS

We perform Monte Carlo (MC) simulations as follows. The calculation starts from a completely bipolar system at low temperatures, with all the particles belonging to the sphere aligned along the local meridian. When available the calculation starts from an already equilibrated configuration at the nearest lower temperature. The Metropolis procedure [28] is then used to update the lattice for a certain number of cycles, i.e., of sets of N attempted moves. Each particle is selected at random for a trial move at every lattice sweep using a random shuffling algorithm [28]. A new trial orientation of the chosen particle is then generated by a controlled variation from the previous one [32]. We have checked that a rejection ratio not too far from 0.5 is achieved while ensuring that an adequate evolution is obtained.

Several thermodynamic observables have been calculated, in particular energy U, dimensionless heat capacity C_V^*, and second- and fourth-rank order parameters,

$\langle P_2\rangle_\lambda$, $\langle P_4\rangle_\lambda$, as obtained from the largest eigenvalue of the ordering matrix [28,33]. We have also calculated a *bipolar order parameter* $\langle P_2\rangle_C$ defined as follows:

$$\langle P_2\rangle_C = \frac{1}{N}\sum_{i=1}^{N} P_2(\mathbf{u}_i\cdot\mathbf{n}_i), \tag{3.1}$$

where $\mathbf{u}_i$ is the orientation vector of the ith particle and $\mathbf{n}_i$ is the local meridian that lies on the plane defined by the droplet axis (z axis) and the radial vector $\mathbf{r}_i$ of the particle while being perpendicular to $\mathbf{r}_i$ itself. $\langle P_2\rangle_C$ thus tends to one for a perfect bipolar structure and in general it quantifies deviations from this organization.

The order parameters introduced are averages performed over all the particles of the sample and, especially at low temperature, they do not, of course, provide any indication of the propagation of the bipolar ordering inside the droplet. To investigate this important aspect we have divided the droplet into a set of concentric shells, in an onion skin fashion [21(b)], and we have calculated the order parameters $\langle P_L\rangle_C$ in these different regions by averaging only over the particles falling within a shell at a distance r from the center.

Another indication of the changing of the molecular organization across the droplet is through the two-particle angular correlation coefficients $G_L(r_{12})$, a set of expansion coefficients of the rotationally invariant pair correlation function [33],

$$G(r_{12},\omega_{12}) = G_0^{00}(r_{12})\sum_L \frac{2L+1}{64\pi^2} G_L(r_{12}) P_L(\cos\beta_{12}). \tag{3.2}$$

The coefficients $G_L(r_{12})$ are, in general, two-particle order parameters

$$G_L(r_{12}) = \frac{1}{G_0^{00}(r_{12})}\int d\omega_1\, d\omega_2\, G(r_{12},\omega_{12})\, P_L(\cos\beta_{12}), \tag{3.3}$$

while $G_0^{00}(r_{12})$ is the radial distribution, that for a lattice simply counts the number of neighbors in progressively larger shells. In a uniform system the $G_L(r_{12})$ for various L give the space correlation of the relative orientation β_{12} of two arbitrary particles separated by a distance r_{12}. Here we wish to investigate the correlation between the orientations of particles at a distance r from the center with those as near as possible to the center itself. In practice for the calculation of pair correlations, the eight particles nearest to the droplet center are selected as origins and the pair correlations with all the other particles within a certain range are calculated. We have calculated the first two angular correlation coefficients $G_2(r)$ and $G_4(r)$ for all the temperatures studied. As already mentioned we wish to investigate two types of effects: the influence of the anchoring strength J [Eq. (2.2)] and that of applied field strength ξ [Eq. (2.3)]. It is clear that for each choice of these parameters a set of temperatures has to be simulated and the number of simulations rapidly becomes overwhelming. Thus to make the whole computer experiment practically feasible a reasonable compromise between the number of temperatures, the sample size, etc., has to be found. In what follows we briefly introduce the set of conditions we have chosen and the results obtained.

A. Anchoring strength effects

We have performed a set of independent simulations with a broad temperature scan for the bipolar boundary condition (BBC) droplet with $N = 304$ particles for five different anchoring strengths, $J = 0.0, 0.25, 0.5, 1.0, 2.0$, and a number of simulations on a larger system, with $N = 1576$ particles, at selected temperatures.

We have shown in our previous papers that such a small sample is sufficient to obtain meaningful qualitative results for the microscopic organization by Monte Carlo simulations [21–23]. This is because the size effects, even though relevant by themselves, are comparatively less important in comparison with the influence of the boundary conditions. We have then examined the effect of varying these boundary conditions by performing a set of simulations at different anchoring strengths (seven values) at two selected temperatures in the ordered and disordered phase.

We notice first that the results for the energy and C_V^* (not shown here for reasons of space) indicate a suppression of the nematic-isotropic (NI) orientational phase transition upon increasing the interaction with the particles at the interface, much as observed for other boundary conditions. We recall that in a bulk nematic system the NI transition is weakly first order at a reduced temperature $T^* = kT/\epsilon = 1.1232$, a behavior roughly approximated also in the simulation of the droplet with $J = 0$ (free boundary). We report in Fig. 1 results for the order parameter $\langle P_2\rangle_\lambda$ that express the order with respect to the instantaneous preferred direction. From these we can see that by increasing the value of the anchoring J the bipolar boundary conditions produce an overall ordering of the system at all temperatures. As the particles follow the surface alignment this parameter becomes less informative; at low temperature it decreases as J increases since the boundary constraint inhibits reaching complete uniform alignment. At high temperatures the system is more ordered when the strength of the bipolar anchoring is stronger and this corresponds to a surface induced paranematic system. This anchoring strength effect is more evident when looking at Figs. 2 and 3 where we present the results for $\langle P_2\rangle_\lambda$ and $\langle P_2\rangle_C$ as a function of the parameter J at two selected temperatures, $T^* = 0.4$ and $T^* = 1.2$, and for the two system sizes. The order parameters $\langle P_2\rangle_\lambda$ and $\langle P_2\rangle_C$ show, of course, an opposite behavior. Moreover the bipolar order parameter $\langle P_2\rangle_C$ loses significance for $J = 0$. All the curves saturate with J and the changes in behavior are relevant approximately up to $J = 2$. Above this value of J the order parameters do not change significantly. We notice that the effect of the boundary conditions cannot overcome the disordering effect of the temperature that does not permit us to reach, at $T^* = 0.4$, a perfect bipolar organization even when an extremely large value of the anchoring parameter J is employed (see Fig. 3).

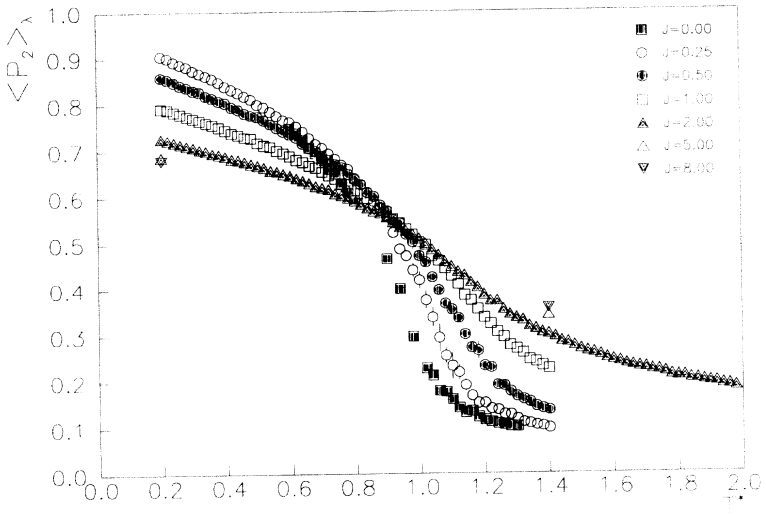

FIG. 1. The second-rank order parameter $\langle P_2 \rangle_\lambda$ for a droplet of 304 particles with bipolar boundary conditions (BBC) as a function of reduced temperature $T^* = kT/\epsilon$. We show results for anchoring strength parameters $J = 0.0, 0.25, 0.5, 1.0, 2.0, 5.0, 8.0$.

B. External field

We now turn to the investigation of the effects of an external field. These effects can possibly be studied experimentally and indeed there have been deuterium NMR experiments, also of bipolar droplets [25], employing electric field alignment. We have previously shown that powder NMR spectra can be calculated from the molecular organizations generated by the simulations [22]. However, we have found it necessary to employ samples of at least 5000 particles to obtain satisfactory NMR spectra. Thus here we have studied a system with 5832 particles. This relatively large sample also allows us to divide the sphere into 11 shells to investigate how the ordering changes starting from the center of the droplet and going towards the surface. On the other hand, because of the nearly 20-fold increase in computer time connected to this larger sample size, we have considered in this case only one value of anchoring strength ($J = 1$) and various values of field coupling ξ ($\xi = -0.5, 0, 0.05, 0.15, 0.3, 0.5$). A further check on size effects has been performed simulating an even larger droplet with $N = 11\,752$ particles in the special case of $J = 1, \xi = 0$.

To estimate the changes in molecular organization produced by a field we find it expedient to consider yet another order parameter, $\langle P_2 \rangle_B$, expressing the molecular alignment with respect to the field

$$\langle P_2 \rangle_B = \frac{1}{N} \sum_{i=1}^{N} P_2(\mathbf{u}_i \cdot \mathbf{B}), \tag{3.4}$$

where $\mathbf{B}$ is the field direction [in the present study we have chosen the field along the $\mathbf{z}$ direction of our laboratory system so $\mathbf{B} = (0, 0, 1)$]. We expect that, at least for a positive susceptivity anisotropy, $\langle P_2 \rangle_B$ should become closer and closer to the value of the usual order parameter $\langle P_2 \rangle_\lambda$ as the field increases. The results for $\langle P_2 \rangle_B$ and $\langle P_2 \rangle_C$ are shown in Figs. 4 and 5, respectively.

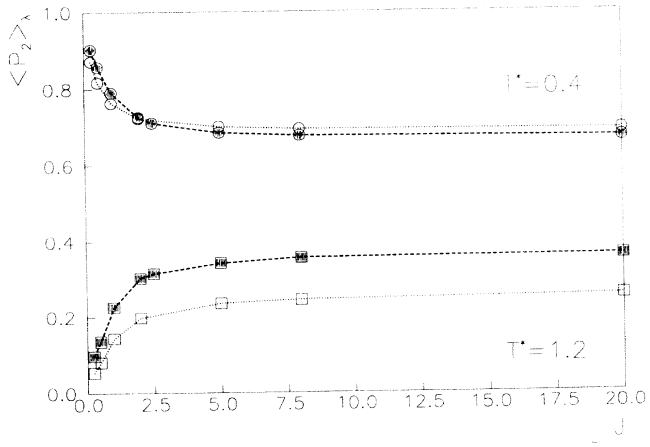

FIG. 2. The second-rank order parameter $\langle P_2 \rangle_\lambda$ for droplets of 304 (full symbols) and 1576 (empty symbols) particles with bipolar boundary conditions (BBC) as a function of the anchoring strength parameter J.

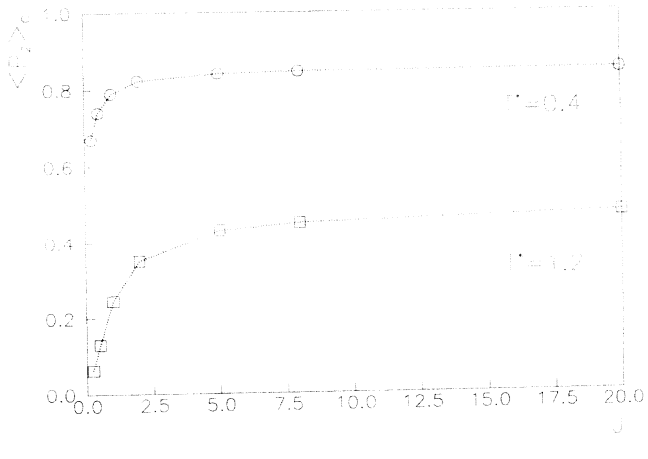

FIG. 3. The bipolar order parameter $\langle P_2 \rangle_C$ for a droplet of 1576 particles with bipolar boundary conditions (BBC) as a function of the anchoring strength parameter J at reduced temperatures $T^* = 0.4, 1.2$.

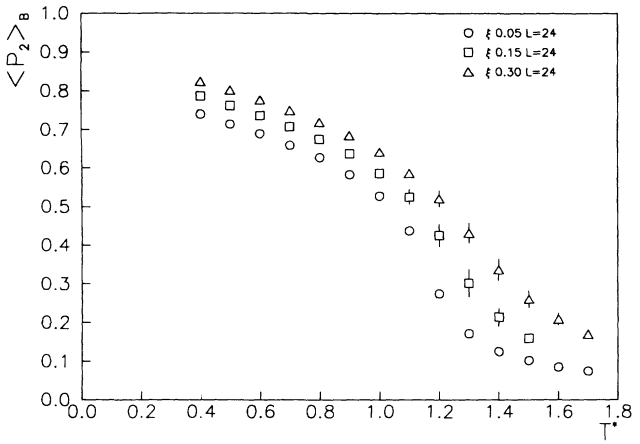

FIG. 4. The second-rank field order parameter $\langle P_2 \rangle_B$ for a droplet of 5832 particles with bipolar boundary conditions (BBC) as a function of reduced temperature. We show results for field strength parameters $\xi = 0.05$ (○), 0.15 (□), and 0.3 (△).

As mentioned before to study the variations of ordering inside the droplet we have calculated the order parameters for particles belonging to regularly spaced shells at various distances from the center. In Fig. 6 we report the results for the order parameters, $\langle P_2 \rangle_\lambda$, $\langle P_2 \rangle_C$, and $\langle P_2 \rangle_B$, versus r at selected temperatures and for three values of ξ. We see at once that $\langle P_2 \rangle_\lambda$ and $\langle P_2 \rangle_B$ become similar for strong fields and positive susceptivity anisotropy, $\xi = 0.5$, as expected. The bipolar order is clearly greater near the surface boundary and its propagation inside the droplet changes with the applied field, being essentially favored when $\xi > 0$ and contrasted by $\xi < 0$. It is interesting to look at the effects of sample size on the order and its propagation. In Fig. 7(a) we have considered the bipolar order for $N = 304, 1472, 5832$, and 11 752 at $T^* = 0.4, \xi = 0.0$ (and $J = 1$ as in Fig. 6) as

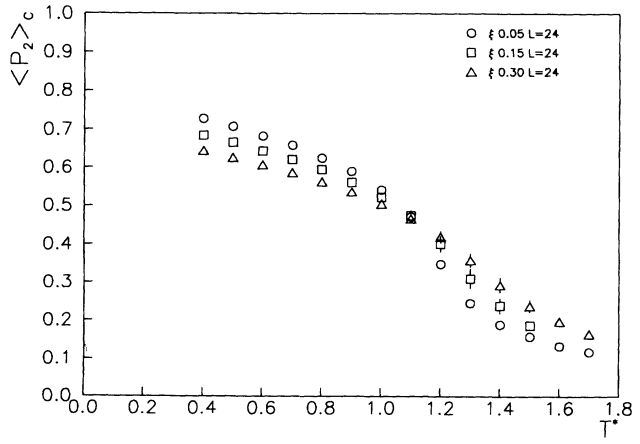

FIG. 5. The bipolar order parameter $\langle P_2 \rangle_C$ for a droplet of 5832 particles with bipolar boundary conditions (BBC) as a function of reduced temperature. We show results for field strength parameters $\xi = 0.05$ (○), 0.15 (□), and 0.3 (△).

a function of r. The first impression is of a rather pronounced change with size. However, it is remarkable to see [Fig. 7(b)] that the curves are essentially superimposable, with some deviation for the smaller droplet, when plotted against the fractional distance (r/r_{max}). This scale invariance seems to suggest that our results for the molecular organization in these rather small assemblies could be transferrable to the much larger sizes often used in experiments on bipolar droplets. The overall results for the radial pair correlation coefficients $G_2(r)$ are presented in Figs. 8(a)–8(c) for three selected temperatures $(T^* = 0.4, 0.9, 1.4)$ and for three values of ξ. In a uniform system the pair coefficients $G_L(r)$ start from one and tail off to essentially the square of the order parameter of rank L, $\langle P_L \rangle^2$ in the nematic phase [33]. Here the situation is quite different, since molecules at the surface have an orientation strongly influenced by the boundary layer of particles with pinned orientations. To understand the behavior of the orientational correlation across the droplet it is useful to write the rotational invariant using an auxiliary laboratory fixed system with the z axis along a certain arbitrary direction $\mathbf{F}$. Thus, applying the spherical harmonics addition theorem,

$$G_L(r_{12}) = \langle P_L(\cos\beta_{12}) \rangle_r \tag{3.5a}$$

$$= \sum_{m=-L}^{L} \langle D^{L*}_{m0}(1-F) D^{L}_{m0}(2-F) \rangle \tag{3.5b}$$

where molecule 1 is near the center of the droplet and the notation $D^L_{m0}(i-F)$ indicates the rotation from frame F to the frame on particle i. At large separation R the orientations of particles 1, 2 become uncorrelated and

$$G_L(R) \approx \sum_{m=-L}^{L} \langle D^{L*}_{m0}(1-F) \rangle \langle D^{L}_{m0}(2-F) \rangle. \tag{3.6}$$

We assume that this is the case for particles at the interface layer so that R corresponds to $r = r_{max} = 12$ and we consider now the three prototype cases of no field and of positive and negative susceptivity anisotropy in turn for the second-rank coefficients $G_2(R)$.

(i) No field ($\xi = 0$). Here we consider $\mathbf{F}$ to be parallel to the director at the center. At low temperatures ($T^* = 0.4$) we then have, thanks to uniaxial symmetry around the director,

$$\langle D^{2*}_{m0}(1-F) \rangle \approx \langle P_2 \rangle_{\lambda,1} \delta_{m0}, \tag{3.7}$$

with $\langle P_2 \rangle_{\lambda,1}$ evaluated at the droplet center and similarly,

$$\langle D^{2*}_{00}(2-F) \rangle \approx \langle P_2 \rangle_{\lambda,R}, \tag{3.8}$$

where $\langle P_2 \rangle_{\lambda,R}$ is now the order at the surface. From Fig. 6 we see that $\langle P_2 \rangle_\lambda \approx 1$ at the center while $\langle P_2 \rangle_\lambda \approx 0.6$ at R. Thus we can expect $G_2(R) \approx 0.6$ and we can see that this is the case in Fig. 8. At high temperatures ($T^* = 1.4$) the situation is different. First of all there is no real director at the center (see the snapshots in Figs. 10–12) and $\langle D^2_{m0}(1-F) \rangle \approx 0$. The surface order parameter is that induced by the boundary conditions ($\langle P_2 \rangle_C \approx 0.2$) and $G_2(R) \approx 0$, as we see again in Fig. 8.

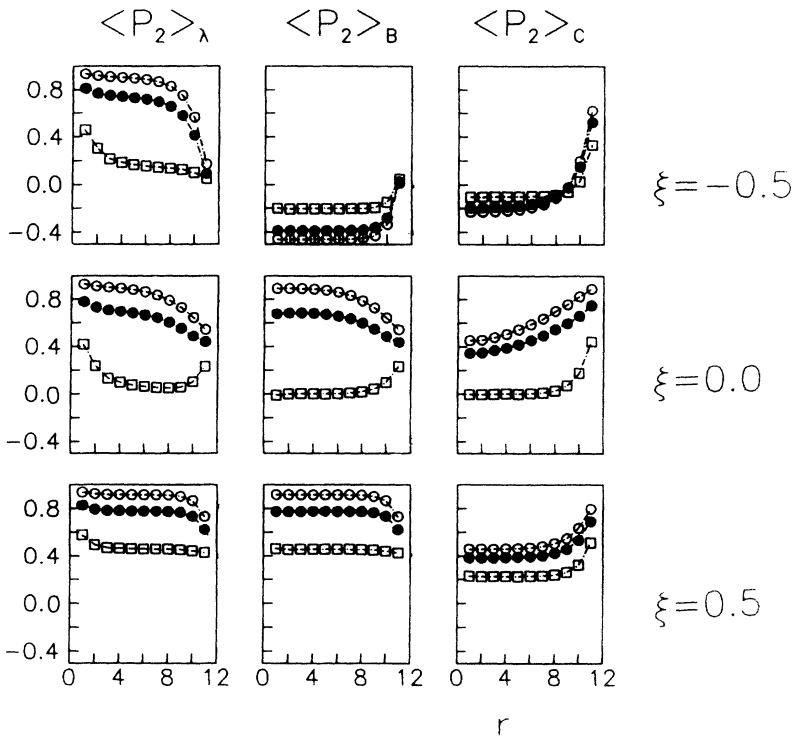

FIG. 6. The second-rank order parameters $\langle P_2\rangle_\lambda$ (left), $\langle P_2\rangle_B$ (center), and $\langle P_2\rangle_C$ (right) against distance from the droplet center in lattice units, r, for three field strengths: $\xi = -0.5$ (top), 0.0 (middle), 0.5 (bottom), and for three different temperatures T^*: 0.4 (○), 0.9 (•), and 1.4 (□)

(ii) Positive susceptivity anisotropy, $\xi = 0.5$. At low temperature the molecules at the center are aligned with the field direction, so we can take in this case the z axis of the arbitrary auxiliary frame F coincident with **B**. Uniaxial symmetry around the field (and the director) now gives

$$\langle D^{2*}_{m0}(1-B)\rangle = \langle P_2\rangle_{B,1}\delta_{m0}. \tag{3.9}$$

From Fig. 6 we see that at $T^* = 0.4$, $\langle P_2\rangle_{B,1} > 0.9$, and $\langle P_2\rangle_{B,R} \approx 0.75$. Thus $G_2(R) \approx 0.7$. At high temperature $\langle P_2\rangle_{B,1} \approx 0.4 - 0.5$ and $\langle P_2\rangle_{B,R} \approx 0.4$. Thus $G_2(R) \approx 0.2$. Once more we see that these expectations are borne out by the results in Fig. 8.

(iii) For the negative susceptivity case, $\xi = -0.5$, the molecules at the center tend to be perpendicular to the field, so that $\langle P_2\rangle_{B,1} \approx -0.4$, approaching the complete order limit of $-\frac{1}{2}$. At the droplet surface $\langle P_2\rangle_{B,R} \approx 0.4$ (Fig. 6) at all temperatures and $G_2(R) \approx 0$.

The fact that we can rationalize the trends in order and correlation in this way indicates that the basic decoupling assumption in Eq. (3.6) for molecules at the center and at the interface holds for our droplet size. Clearly we expect these results to hold also for large droplets.

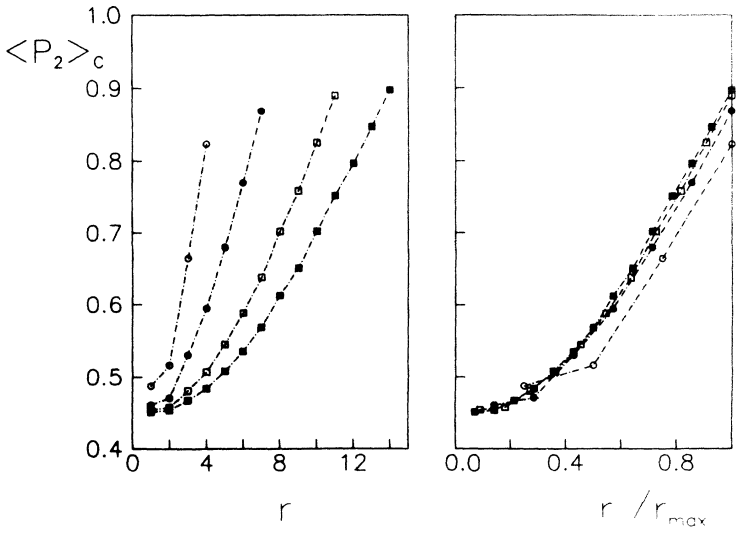

FIG. 7. The second-rank order parameters $\langle P_2\rangle_C$ against distance in lattice units, r, (left) and scaled distance r/r_{max} (right) for four different sizes of the droplet: $N = 304$ (○), $N = 1576$ (•), $N = 5832$ (□), and $N = 11752$ (■). Here $\xi = 0.0$ and $T^* = 0.4$.

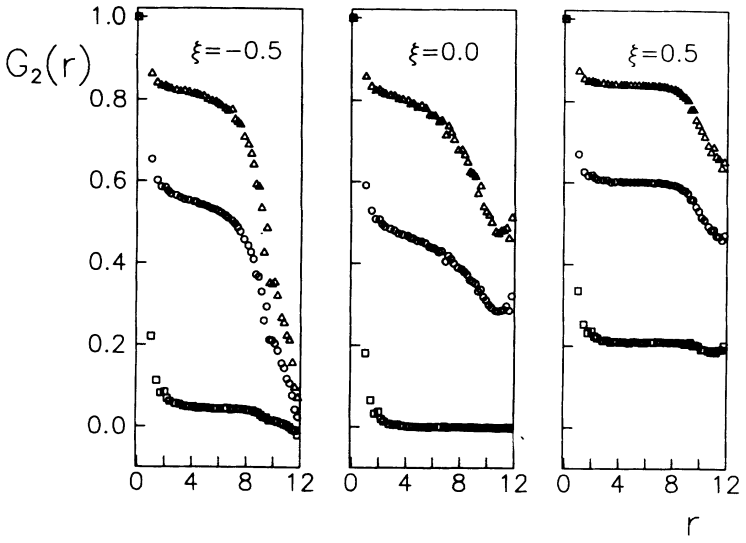

FIG. 8. The second-rank radial correlation coefficient $G_2(r)$ plotted against r in lattice units as obtained from the MC simulation with $N = 5832$ particles at $T^* = 0.4$ (△), 0.9 (○), and 1.4 (□). The results for three field strengths $\xi = -0.5$, $\xi = 0.0$, and $\xi = 0.5$ are shown.

C. Deuterium powder NMR spectra

Deuterium NMR of deuterated liquid crystals has become the technique of choice for studying PDLC droplets [25,34]. The use of ^{2}H NMR allows focusing on the molecules inside the droplet (the only ones to be deuterated) thus giving in principle a direct handle on their properties. The spectrum will depend on the time scale of spins changing from one ordered domain to another. In the limit of very fast motion an average is obtained giving a single peak spectrum with limited information on the underlying molecular organization. The other, static, limit of domain motion frozen on the experimental time scale is perhaps more interesting and here we present calculations of static NMR line shapes. From the simulation results, or more precisely from the instantaneous configurations given as a set of direction cosines, we have calculated the polydomain deuterium NMR line shapes for a system of fictitious molecules with an axis of effective molecular uniaxial symmetry corresponding to the $\mathbf{u}_i$ obtained for our configurations. For simplicity, we shall discuss this as if one site corresponded to one molecule. However this experiment cannot distinguish between the case of a cluster of molecules with effective uniaxial symmetry and local orientation given by our "spins." Thus in practice we use the procedure described in detail in [22]. The powder NMR spectrum is simulated as an average, over a number of configurations sufficient to give convergence, of the instantaneous spectra calculated by summing the doublet type of contribution coming from each site in the sample.

In practice, the NMR line shapes are calculated from an average of over ten droplet configurations of the large ($N = 5832$) droplets using parameters appropriate to 4′-methoxy-4-cyanobiphenyl-d_3 (10CB) [22,34]. Spectra obtained at different field strengths and at three temperatures are given in Figs. 9–11 together with some typical snapshots at the same temperatures. We consider first the zero field, $\xi = 0$, case (Fig. 10). At $T^* = 0.4$ the bipolar configuration dominates (see snapshots) and gives an effective aligned spectrum with a doublet structure. Notice that in a similar study with radial boundary conditions (RBC) we have found a rather different, powderlike, spectrum at $\xi = 0$, showing that the two organizations can be distinguished by NMR. This was experimentally demonstrated by Golemme *et al.* [34]. With BBC the powder spectrum is only recovered at high temperature where the disorder overcomes the effect of the boundaries.

As the field strength increases a sharper doublet structure is obtained both with positive and negative ξ (Fig. 9 and Fig. 11). With $\xi < 0$ the doublet spacing is half of the one with $\xi > 0$ as expected from purely geometric reasons. At high temperature a different behavior, which can be rationalized from the three dimensional (3D) isotropiclike spectrum at $\xi = 0$, is found. Thus for $\xi < 0$ the effect of the field is to enhance the inner, perpendicular lines that then appear more visible. On the contrary, for $\xi > 0$ intensity is subtracted from this central doublet and a rather flat pattern results. It is interesting to notice that the spectrum obtained at $T^* = 0.4$, $\xi = 0$ for $N = 11\,572$ particles is superimposable with that calculated with $N = 5832$ showing once more that our results should be applicable to larger droplets as well.

D. Simulated polarized light experiments

Given that the results for our small droplet seem to be applicable to larger ones it is tempting to see if the scale invariance can be pushed to micrometer sized droplets which actually could have been investigated using polarized light microscopy (sizes of at least $2-3$ μm are needed [35]). In this case a scale factor of the order 10^2 would have to be invoked, at least for low molar mass nematic droplets. While this seems to represent a rather bold assumption to hold, it is interesting to calculate what the optical textures would be scaling up our MC configurations.

In practice the calculation is performed using a standard matrix approach as employed by various workers, e.g., Ondris-Crawford *et al.* [35], Xu *et al.* [36], and Kilian [37] in their calculations based on continuum theory. The incoming light is represented as a four components

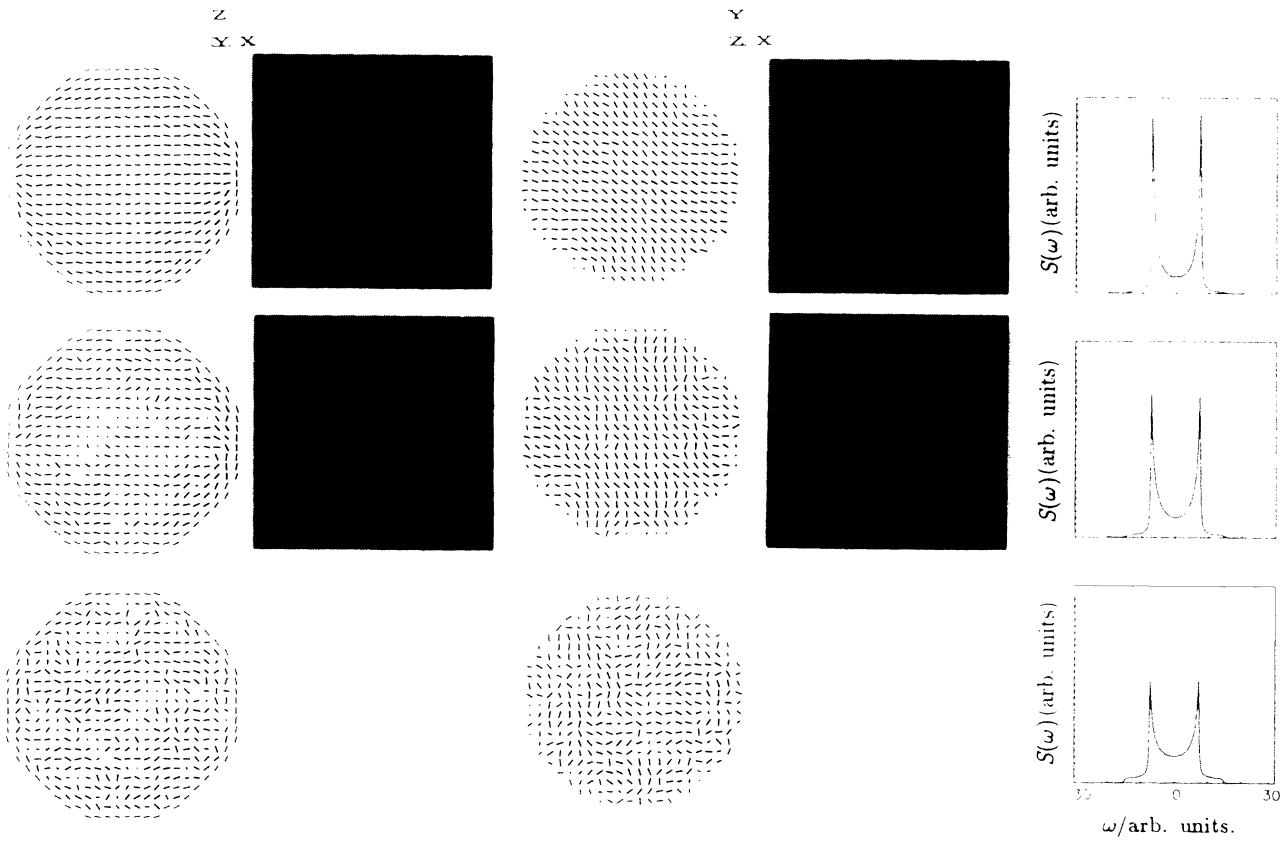

FIG. 9. Snapshots (vertical and equatorial sections) and static polydomain deuterium NMR line shapes for three temperatures [$T^* = 0.4$ (top), 0.9 (middle), and 1.4 (bottom)] for field strength $\xi = -0.5$. We also report optical patterns for the two lower temperatures for the same field strength.

Stokes vector. The basic assumption is that ray optics can be used and that each site in the droplet is described by a Müller matrix. The light beam going through a row of particles across the droplet is then retarded by the matrix resulting from the product of the Müller matrices for each particle in the light path. The Müller matrix for particle j, which corresponds to a simple linear retarder, is then given by [38]

$$\mathbf{M}_j = \begin{pmatrix} 1 & 0 & 0 & 0 \\ 0 & \sin^2 2\phi_j + \cos^2 2\phi_j \cos\delta_j & -\cos 2\phi_j \sin\delta_j & \sin 2\phi_j \cos 2\phi_j (1-\cos\delta_j) \\ 0 & \cos 2\phi_j \sin\delta_j & \cos\delta_j & -\sin 2\phi_j \sin\delta_j \\ 0 & \sin 2\phi_j \cos 2\phi_j (1-\cos\delta_j) & \sin 2\phi_j \sin\delta_j & \cos^2 2\phi_j + \sin^2 2\phi_j \cos\delta_j \end{pmatrix}, \tag{3.10}$$

where ϕ_j is the angle between the projection of the axis of the particle on the plane perpendicular to the direction of the light and the y axes or z axes, respectively, depending on the incoming light being parallel to the z or the y axes. The phase difference δ_j of the particle j is defined as [36]

$$\delta_j = 2\pi \frac{h}{\lambda} n_0 \left(\frac{n_e}{n_{e,j}} - 1 \right) \tag{3.11}$$

where $h = 2R/L$ is the thickness of the layer, L is the number of layers, i.e., in our case the maximum number of particles in the droplet that a light beam encounters, and λ is the wavelength of the light. n_0 is the ordinary refractive index of the liquid crystal. The effective extraordinary refractive index, $n_{e,j}$ is obtained from

$$n_{e,j} = \sqrt{n_0^2 + (n_e^2 - n_0^2)\cos^2\theta_j}, \tag{3.12}$$

where n_e is the parallel component of the effective refractive index and θ_j is the angle between the axis of the jth particle and the direction of propagation of the light.

The resulting Stokes vector of the polarized and retarded light beam is thus given by [36,38]

$$\mathbf{s} = \mathbf{P}_{out} \Pi_j \mathbf{M}_j \mathbf{P}_{in} \mathbf{s}_{in}, \tag{3.13}$$

where

$$\mathbf{s}_{in} = \begin{pmatrix} 1 \\ 0 \\ 0 \\ 0 \end{pmatrix}$$

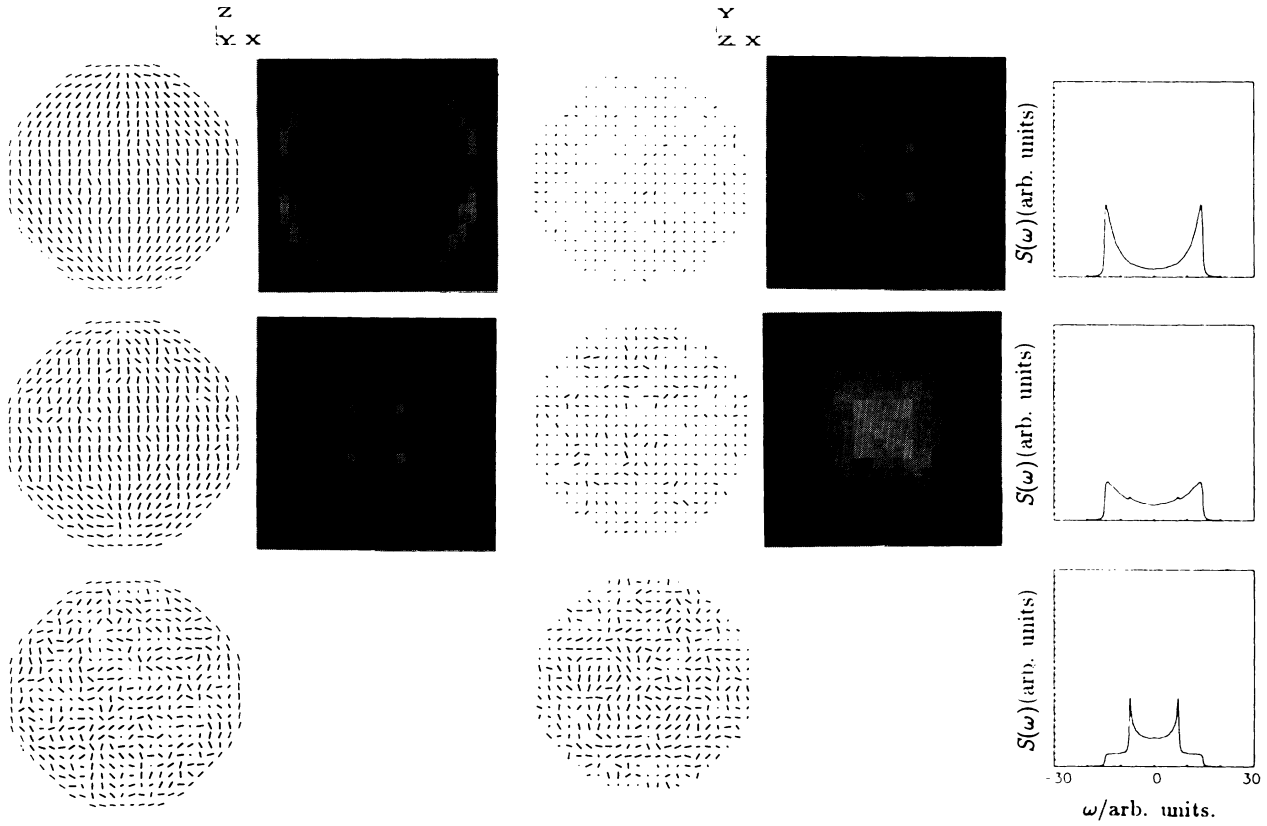

FIG. 10. Same as Fig. 9 for field strength $\xi = 0.0$.

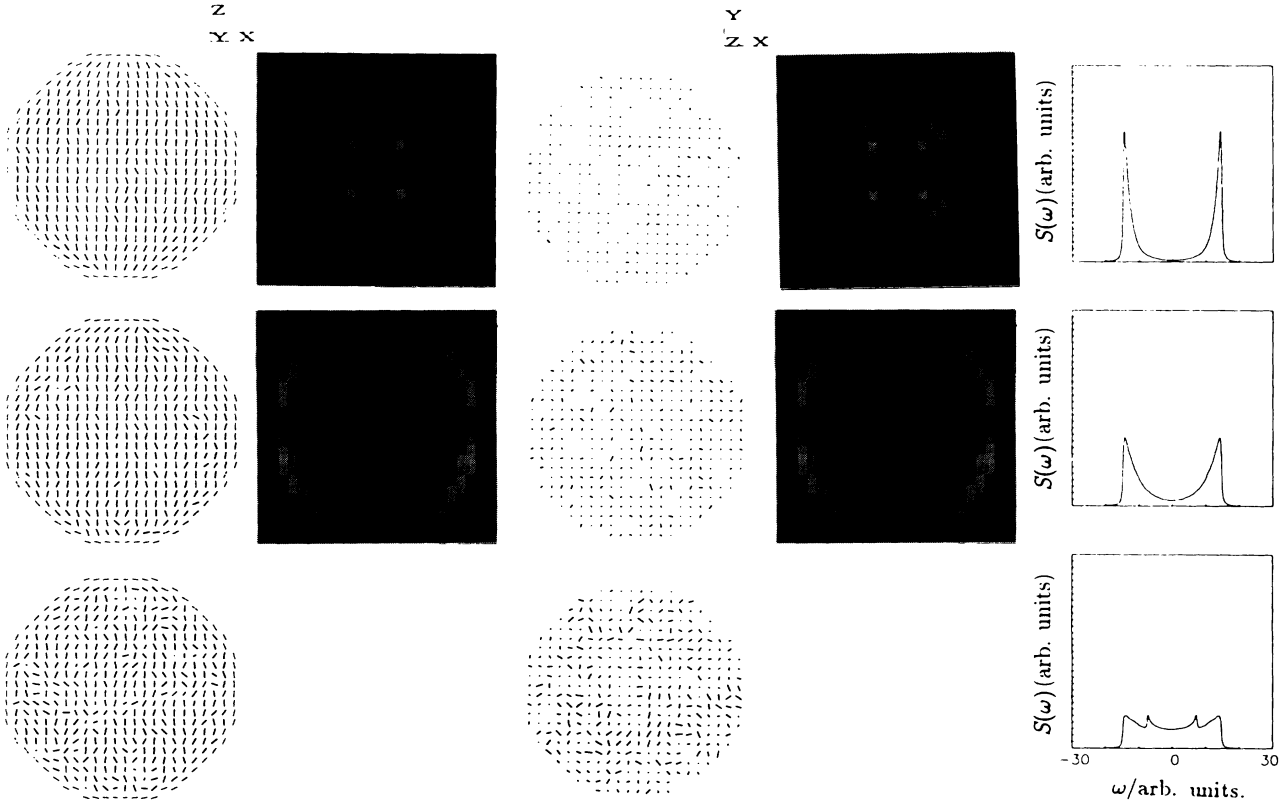

FIG. 11. Same as Fig. 9 for field strength $\xi = 0.5$.

corresponds to the Stokes vector of unpolarized light, and $\mathbf{P}_{in}$ and $\mathbf{P}_{out}$ are Müller matrices representing the polarizer and the analyzer, respectively. In our calculations the Müller matrix representing the crossed polarizer and analyzer [38] is defined as

$$\mathbf{P}_{0,90} = \frac{1}{2}\begin{pmatrix} 1 & 0 & 0 & \pm 1 \\ 0 & 0 & 0 & 0 \\ 0 & 0 & 0 & 0 \\ \pm 1 & 0 & 0 & 1 \end{pmatrix}. \tag{3.14}$$

The intensity is proportional to the first element in the output Stokes vector **s**. If

$$\mathbf{s} = \begin{pmatrix} s_0 \\ s_1 \\ s_2 \\ s_3 \end{pmatrix}$$

then the intensity $I \propto s_0$ and $s_0^2 \geq s_1^2 + s_2^2 + s_3^2$. To improve the signal to noise ratio of the image resulting from the simulated droplet configurations we have averaged over N_C equilibrated configurations, so we actually use the expression

$$\mathbf{s} = \mathbf{P}_{90}\frac{1}{N_C}\sum_{N_C}\left(\prod_j \mathbf{M}_j^{(N_C)}\mathbf{P}_0\mathbf{s}_{in}\right). \tag{3.15}$$

The intensity is thus calculated as a projection in the plane perpendicular to the light propagation. An image of a configuration obtained from a $22 \times 22 \times 22$ lattice, which corresponds to a sphere with 5832 particles, gives a picture of 22×22 pixels with intensity coded in a scale from black, no light, to white, full intensity, with 32 different gray levels. We have normalized the gray levels in each picture so as to vary from white to black for the highest and lowest intensity, respectively.

In practice the angles ϕ_j and θ_j, describing the position of a particle j, are taken from the simulated droplet configurations and the following values of the parameters have been used in the calculations: the layer thickness, $h = (5.3\ \mu\text{m})/L$; the wavelength, $\lambda = 545$ nm; the ordinary refractive index, $n_o = 1.5$; and the extraordinary refractive index, $n_e = 1.7$. We have arbitrarily taken these refractive indices to be constant with temperature, since we assume that the local domain basically remains unchanged and the simulation describes only the disordering of the domains with respect to each other. These parameters resemble those of the nematic liquid crystal 5CB [35]. We report in Figs. 9–11 a summary of results for the three applied field situations and for the two lower temperatures where the present assumptions are more appropriate. We show vertical and horizontal sections of the microscopic organization as viewed from the x and z axes respectively. We also show optical textures between crossed polarizers for light traveling along these two directions. Notice that the relative gray scales used overemphasize the nonuniformity across the droplet. This is effective for the low temperature cases but can be somewhat misleading at higher temperatures. Even with the limited resolution due to the small number of pixels available, it is comforting to see that the textures obtained seem to be in substantial agreement with the ones obtained experimentally or calculated with continuum theory, when these are available for comparison [35,38]. In Fig. 12 we show snapshots of different droplet sizes ($N = 304, 5832$, and 11 752) together with corresponding optical textures viewed from the z axis. We see that, in agreement with our argument of scale invariance, the polarized light pattern is qualitatively repeated in the three images.

IV. CONCLUSION

We have studied, using the MC method, a model of PDLC's with bipolar boundary conditions. We have determined the microscopic organizations inside the droplets at various temperatures and for various anchoring strengths. We have also studied the effect of an applied field, both with a positive and a negative susceptivity anisotropy. The variety of organizations obtained is rationalized looking at the ordering profile across the

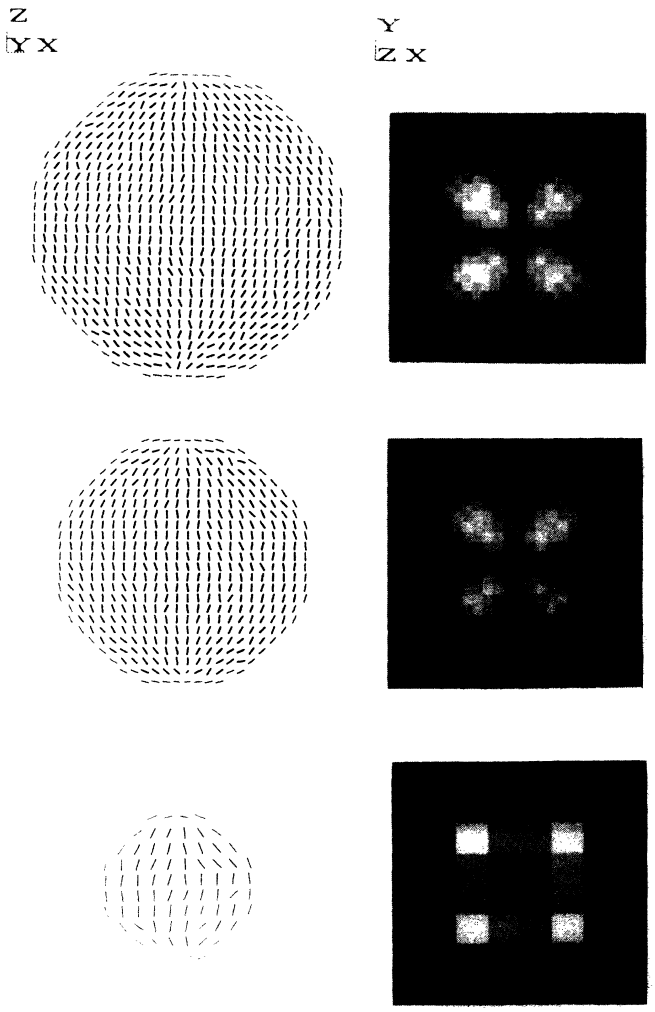

FIG. 12. Snapshots and simulated textures between crossed polarizers of droplet configurations for three different drop sizes, $N = 11\,752$ (top), $N = 5832$ (middle), and $N = 304$ (bottom) at $T^* = 0.4$ and $\xi = 0.0$. We show a vertical section for the snapshots and the optical textures viewed along the z axis.

droplet, and contact with experiment is realized in terms of simulated deuterium NMR spectra and of polarized optical textures. The techniques proposed here seem powerful enough to predict the behavior of the complicated systems in a variety of situations of fundamental and practical interest.

ACKNOWLEDGMENTS

We are grateful to MURST and CNR for support in particular through P.F. "Sistemi Informatici e Calcolo Parallelo" S.P.1. We also acknowledge help from Dr. P. Mazzanti. E.B. thanks the Swedish NFR and EEC HCM.

[1] J.W. Doane, N.A. Vaz, B.-G. Wu, and S. Žumer, Appl. Phys. Lett. **48**, 269 (1986).
[2] G.P. Crawford and J.W. Doane, Condens. Matter News **1**, 5 (1992).
[3] P.S. Drzaic, J. Appl. Phys. **60**, 2142 (1986).
[4] A. Golemme, S. Žumer, D.W. Allender, and J.W. Doane, Phys. Rev. Lett. **61**, 2937 (1988).
[5] G.E. Volovik and O.D. Lavrentovich, Zh. Eksp. Teor. Fiz. **85**, 1997 (1983) [Sov. Phys. JETP **56**, 1159 (1983)].
[6] R.D. Williams, J. Phys. A **19**, 3211 (1986).
[7] P.S. Drzaic, Mol. Cryst. Liq. Cryst. **154**, 289 (1988).
[8] R.D. Sherman, Phys. Rev. A **40**, 1591 (1989).
[9] S. Kralj and S. Žumer, Phys. Rev. A **45**, 2461 (1992).
[10] J. Bezic and S. Žumer, Liq. Cryst. **11**, 593 (1992).
[11] G.P. Crawford, J.A. Mitcheltree, E.P. Boyko, W. Fritz, S. Žumer, and J.W. Doane, Appl. Phys. Lett. **60**, 3226 (1992).
[12] A. Scharkowski, G.P. Crawford, S. Žumer, and J.W. Doane, J. Appl. Phys. **73**, 7280 (1993).
[13] R.D. Polak, G.P. Crawford, B.C. Kostival, J.W. Doane, and S. Žumer, Phys. Rev. E **49**, 978 (1994).
[14] B.J. Liang and Shu-Hsia Chen, Jpn. J. Appl. Phys. **30**, L1955 (1991).
[15] B.J. Liang and Shu-Hsia Chen, J. Appl. Phys. **71**, 2189 (1992).
[16] R. Ondris-Crawford, G.P. Crawford, J.W. Doane, S. Žumer, M. Vilfan, and I. Vilfan, Phys. Rev. E **48**, 1998 (1993).
[17] G.P. Crawford, D.W. Allender, and J.W. Doane, Phys. Rev. A **45**, 8693 (1992).
[18] R. Ondris-Crawford, G.P. Crawford, S. Žumer, and J.W. Doane, Phys. Rev. Lett. **70**, 194 (1993).
[19] S. Žumer, M. Vilfan, and I. Vilfan, Liq. Cryst. **3**, 947 (1988).
[20] N. Schopohl and T.J. Sluckin, J. Phys. **49**, 1097 (1988).
[21] (a) C. Chiccoli, P. Pasini, F. Semeria, and C. Zannoni, Phys. Lett. A **150**, 311 (1990); (b) Mol. Cryst. Liq. Cryst. **212**, 197 (1992).
[22] (a) E. Berggren, C. Zannoni, C. Chiccoli, P. Pasini, and F. Semeria, Chem. Phys. Lett. **197**, 224 (1992); (b) Phys. Rev. E **49**, 614 (1994).
[23] C. Chiccoli, P. Pasini, F. Semeria, and C. Zannoni, Mol. Cryst. Liq. Cryst. **221**, 19 (1992).
[24] I. Vilfan, M. Vilfan, and S. Žumer, Phys. Rev. A **40**, 4724 (1989).
[25] R. Aloe, G. Chidichimo, and A. Golemme, Mol. Cryst. Liq. Cryst. **203**, 1155 (1991).
[26] C. McFarland, J.L. Koenig, and J.L. West, Appl. Spectrosc. **47**, 598 (1993).
[27] P.A. Lebwohl and G. Lasher, Phys. Rev. A **6**, 426 (1972).
[28] U. Fabbri and C. Zannoni, Mol. Phys. **58**, 763 (1986).
[29] G.R. Luckhurst and C. Zannoni, Nature (London) **267**, 412 (1977).
[30] R. Berardi, A. Emerson, and C. Zannoni, J. Chem. Soc. Faraday Trans. **89**, 4069 (1993).
[31] G.R. Luckhurst, P. Simpson, and C. Zannoni, Chem. Phys. Lett. **78**, 429 (1981).
[32] J.A. Barker and R.O. Watts, Chem. Phys. Lett. **3**, 144 (1969).
[33] C. Zannoni, *The Molecular Physics of Liquid Crystals,* edited by G.R. Luckhurst and G.W. Gray (Academic, London, 1979), Chap. 9, p. 191.
[34] A. Golemme, S. Žumer, J.W. Doane, and M.E. Neubert, Phys. Rev. A **37**, 559 (1988).
[35] R. Ondris-Crawford, E.P. Boyko, B.G. Wagner, J.H. Erdmann, S. Žumer, and J.W. Doane, J. Appl. Phys. **69**, 6380 (1991).
[36] F. Xu, H.-S. Kitzerow, and P.P. Crooker, Phys. Rev. A **46**, 6535 (1992).
[37] A. Kilian, Liq. Cryst. **14**, 1189 (1993).
[38] J.A. Schellman, *Polarized Spectroscopy of Ordered Systems,* edited by B. Samori' and E.W. Thulstrup (Kluwer, Dordrecht, 1988), p. 231.

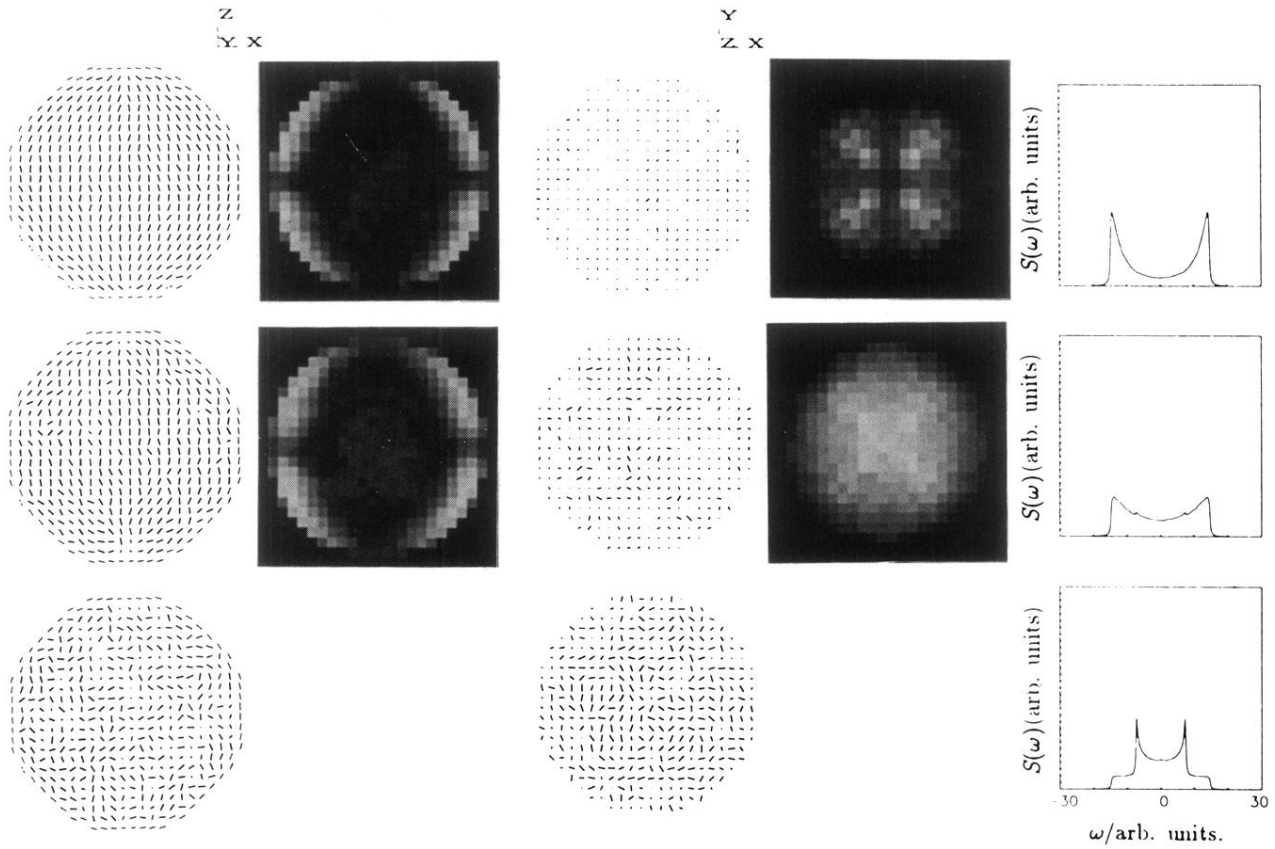

FIG. 10. Same as Fig. 9 for field strength $\xi = 0.0$.

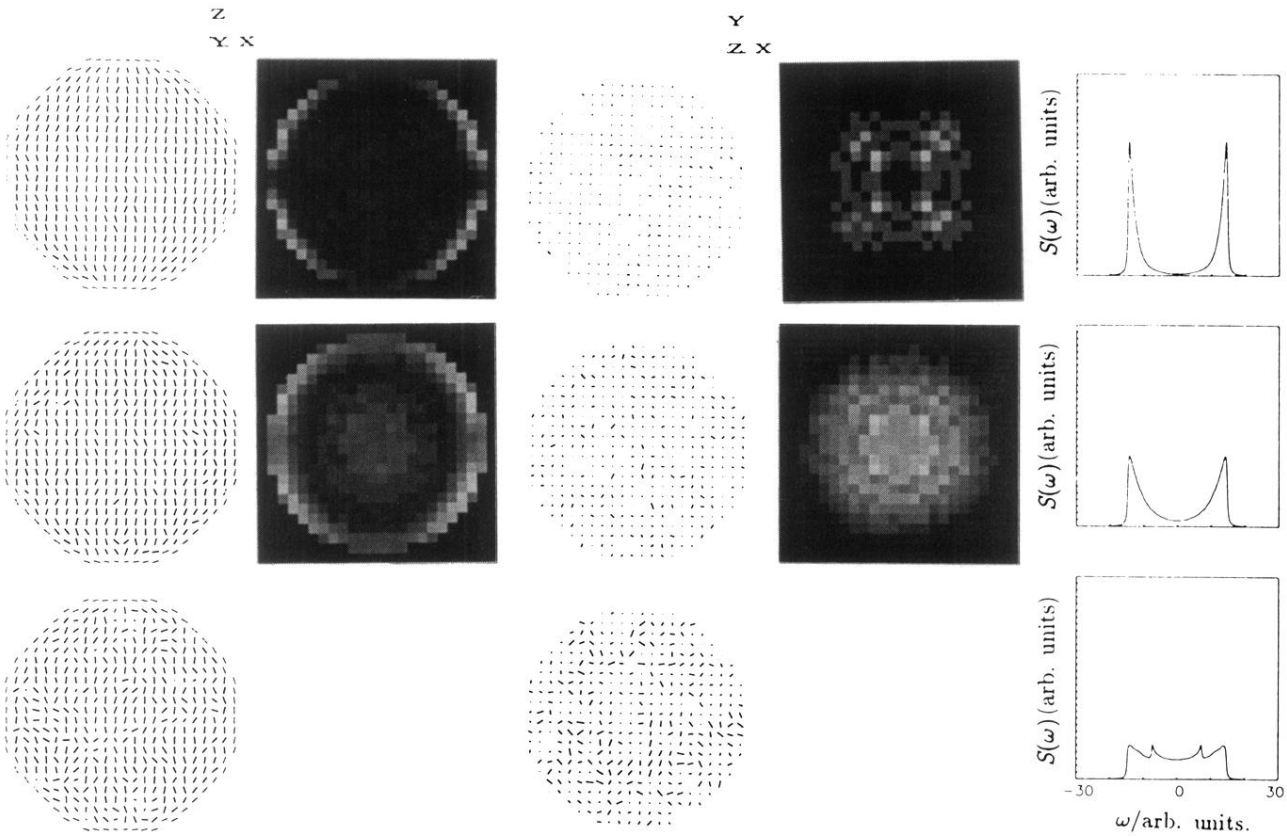

FIG. 11. Same as Fig. 9 for field strength $\xi = 0.5$.

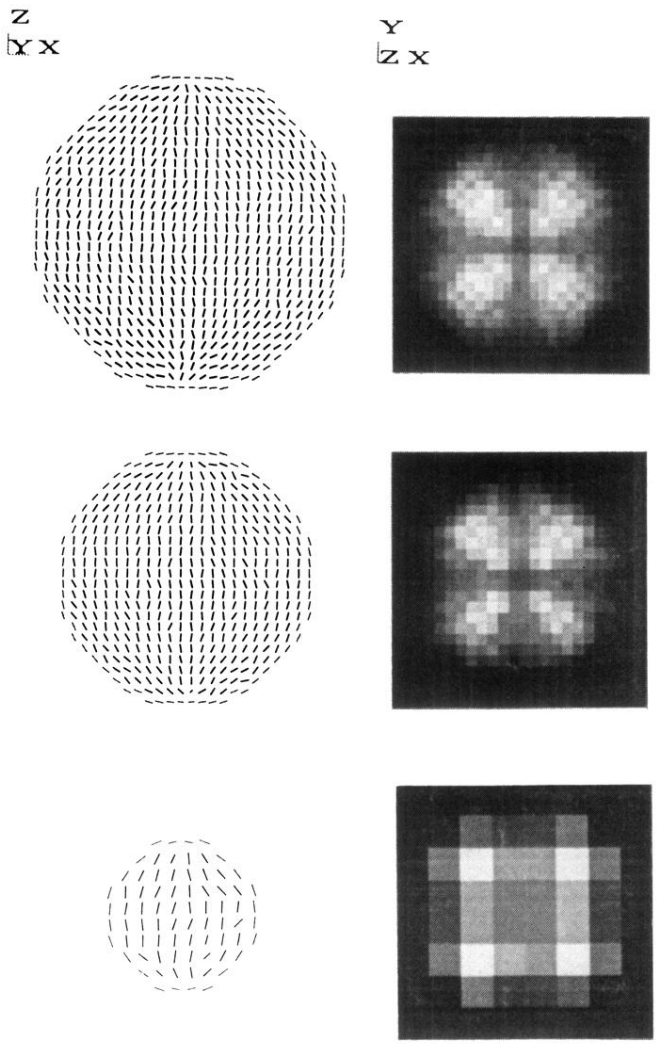

FIG. 12. Snapshots and simulated textures between crossed polarizers of droplet configurations for three different drop sizes, $N = 11\,752$ (top), $N = 5832$ (middle), and $N = 304$ (bottom) at $T^* = 0.4$ and $\xi = 0.0$. We show a vertical section for the snapshots and the optical textures viewed along the z axis.

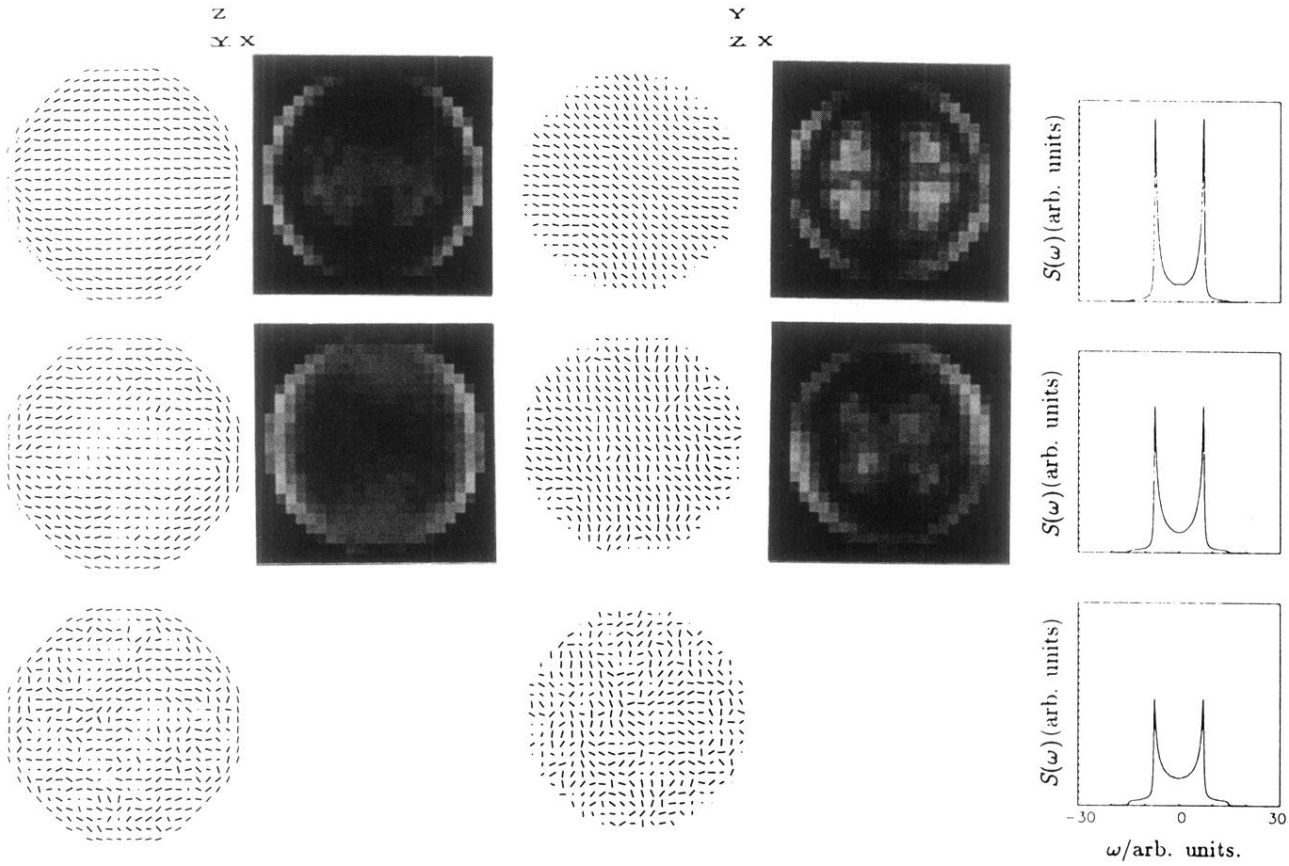

FIG. 9. Snapshots (vertical and equatorial sections) and static polydomain deuterium NMR line shapes for three temperatures [$T^* = 0.4$ (top), 0.9 (middle), and 1.4 (bottom)] for field strength $\xi = -0.5$. We also report optical patterns for the two lower temperatures for the same field strength.